Macromolecules

Cite This: Macromolecules 2018, 51, 9405−9411

Article

pubs.acs.org/Macromolecules

Multiresponsive, Critical Gel Behaviors of Polyzwitterion−Polyoxometalate Coacervate Complexes

Benxin Jing,*[,†] Donghua Xu,[‡] Xiaorong Wang,[§] and Yingxi Zhu*[,†]

[†]Department of Chemical Engineering and Materials Science, Wayne State University, Detroit, Michigan 48202, United States

[‡]State Key Laboratory of Polymer Physics and Chemistry, Changchun Institute of Applied Chemistry, Chinese Academy of Sciences, Changchun, Jilin, China

[§]School of Chemical Science and Engineering, Tongji University, Shanghai, China

Supporting Information

ABSTRACT: Macromolecular coacervate complexation via spontaneous liquid−liquid separation has become a facile supramolecular assembly approach to produce new functional nanomaterials in aqueous media. Distinct from conventional polyelectrolyte coacervates, the coacervate complexes formed between net neutral zwitterionic polymers and inorganic anionic nanometer-scaled polyoxometalates (POMs) in salted solutions exhibit unique salt hardening and critical gel behaviors with significantly enhanced viscoelasticity due to added POMs. Rheology and fluorescence recovery after photobleaching (FRAP) results suggest that POM macroions not only participate in coacervate complexation but also work as cross-linkers to modulate the stimuli-responsive gel-like microstructure, yielding an optimal POM-to-polyzwitterion molar ratio for the most stable and strongest coacervate complexation. Importantly, the viscoelastic strength and mesh pore size of gel-like coacervate complexes can be tuned over several orders of magnitude by POM and salt concentrations and temperature, which offers unprecedentedly high tunability to tailor the material properties of polymer−POM coacervate complexes for practical applications.

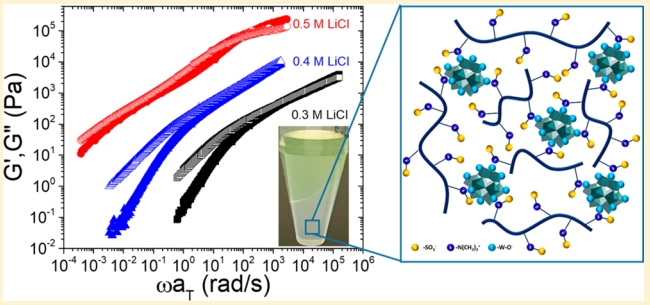

INTRODUCTION

Macromolecular coacervate complexes, which are self-associative liquid−liquid separating materials, have attracted increasingly interest in the recent two decades since the first reported Agar−gelatin coacervate formation in the late 1890s.[1] Biological coacervate complexes can be found in living cells[2] and in the organisms of sandcastle worm, mussel, and tubeworm[3−5] and are also linked to the protocell evolution for the origin of life.[6,7] They have exhibited an array of unique material properties, such as ultralow interfacial tension,[8] extremely high elongation under stress,[3] and superhigh adhesive fracture energy.[9] Biomimetic coacervate complexes have been developed as underwater adhesives,[10] supramolecular self-assembly,[11,12] self-healing hydrogels,[13] drug/gene delivery,[14] and artificial protocells.[15,16] Synthetic coacervate complexes have been mainly formed between oppositely charged polyelectrolytes, including proteins, DNAs, and other charged polymers. Given the right concentration and charge density of charged macromolecules and salt concentration, a variety of binary macromolecular mixtures can spontaneously separate into two immiscible aqueous phases consisting of one polymer-rich phase as dense coacervate and the other polymer-poor phase as supernatant.[17−19] However, as most recent researches have focused on the thermodynamic origin and phase diagram of polyelectrolyte coacervate complexation,[17−20] tunable material properties of coacervate complexes remain poorly achieved, possibly due to their unclear and debated microstructures.

For various practical applications, it is highly desired to design and control multistimuli-responsive coacervate complexes with tunable structural and mechanical properties. The living organisms of mussels and sandcastles in the form of coacervate complex can resist considerably high mechanical deformation and exhibit reversible structural changes in response to various environmental stimuli.[5,9] Conversely, the knowledge and capability of effective control and modification of synthetic coacervate complexes remain rather limited. In this work, we have adopted a simple nanocomposite approach to investigate highly tunable, stimuli-responsive coacervate complexes formed between zwitterionic polyelectrolytes and inorganic multivalent POM macroions in salted aqueous solution. Such hybrid organic−inorganic macroion coacervate nanocomplexes could provide great promise for molecular design of "smart" functional composite nanomaterials.[21−23] Polyelectrolytes have been demonstrated superior to neutral materials[24] to the extent of stimuli-responsive swelling, ion transport, and lubrication as well as their striking similarities with many biological membranes, such as those found in

Received: August 15, 2018
Revised: October 25, 2018
Published: November 14, 2018

DOI: 10.1021/acs.macromol.8b01759
Macromolecules 2018, 51, 9405−9411

mitotic chromosomes, corneas, and jellyfish.[25,26] Recently, we have explored multivalent nanometer-scaled POMs of 0.8−3 nm in diameter as the inorganic polyanions to demonstrate the generality of zwitterion−anion ion pairing induced macroion coacervate complexation with zwitterionic polyelectrolytes.[27] POMs are the clusters of transition metal oxides,[9] $\{MO_n\}$ where n = 4−7 and M is generally Mo, W, V, U, and Nb in well-defined crystalline structures and often carry stable and well-defined multiple negative charges in aqueous solution.[28,29] Because of their unique chemical, optical, and electrical properties, POMs have emerged as novel functional nanomaterials used for catalysis,[30,31] semiconductors,[32] and anticancer/virus and antiamyloid treatments.[33,34] Introducing inorganic POMs to stimuli-responsive polyelectrolytes toward hybrid organic−inorganic macroion coacervate complexation can not only modify the mechanical properties of coacervate complexes[21−23] but also integrate new functions from both polyelectrolytes and POMs to expand their applications.

We have recently demonstrated the entropy-driven coacervate formation between zwitterionic poly(sulfobetaine methacrylamide) (PSBMA) bearing net zero charge and inorganic polytungstate $\{W_{12}\}$ ($Li_6H_2W_{12}O_{34}$) bearing eight negative charges per $\{W_{12}\}$ in LiCl aqueous solutions based on zwitterion−anion pairing as their molecular structures are illustrated in Figure 1a.[27] It should be noted that our POM−polyzwitterion coacervate is mechanistically different from previously reported POM-net positively charged gelatin coacervates or hydrogels based on conventional anion−cation pairing.[21−23] Because of high disparity in their charge density, size, and molecular rigidity of PSBMA and $\{W_{12}\}$, non-stoichiometric PSBMA−$\{W_{12}\}$ coacervate complexes can be formed over a broad range of the molar ratio of total $\{W_{12}\}$ charges (= 8 × $\{W_{12}\}$ molar concentration) to total PSBMA monomers, $c_{e\{W12\}}/c_{SBMA}$ = 80−220% at LiCl concentration c_{LiCl} = 0.5 M, deviating from ∼100% for apparent charge neutrality. Zwitterionic PSBMA becomes effectively net negatively charged in $\{W_{12}\}$-added aqueous solution and exhibits higher negativity than that in simple salted solutions, strongly suggesting the binding of $\{W_{12}\}$ polyanions to PSBMA to replace and release bound monovalent Cl^- anion in LiCl solution for the PSBMA−$\{W_{12}\}$ coacervate complexation. Also increasing salt concentration can broaden the PSBMA−$\{W_{12}\}$ coacervate phase regime in an opposite trend to that of conventional polyelectrolyte coacervates.[17−20] Yet it remains unclear of how the stimuli-responsive characteristics of PSBMA in aqueous solution is modified upon coacervate complexation.[35] More critically, the microstructure of polyelectrolyte coacervates is rather unclear and debated. Recent linear rheology study of polyelectrolyte−protein coacervate complexes suggests a polyelectrolyte network with bound proteins as transient cross-linkers through dynamic ion-pairing.[36] With the "network" model, the viscoelastic strength and stress relaxation of coacervate complexes could be modified by ion-pairing strength with added salts.[37] Yet this model has been challenged by the "mesophase" model, where two microdomains exist:[18] polyelectrolytes and proteins exhibit fast and slow diffusion dynamics in the dilute and dense microdomains, respectively, where the fast diffusion resembles the diffusive dynamics of proteins or molecular probes in dilute polymer solution or in the supernatant of coacervate complexes. However, the "mesophase" model can be questioned as the submicrometer sized microdomains are not observed directly by optical or fluorescence microscopy. A more recent study by X-ray scattering and rheology reports that the polyelectrolyte dense coacervates behave like semi-dilute polyelectrolyte solution.[38] Nevertheless, the debated microstructures of dense coacervate complexes could be highly system-dependent and might be impacted by the enthalpic contribution from intermolecular interaction. In this work, we focus on tuning and understanding the microstructure of PSBMA−$\{W_{12}\}$ dense coacervates against varied solution conditions. Specifically, linear rheology and FRAP characterizations are performed to examine the stimuli-responsive microstructures and viscoelasticity of PSBMA−$\{W_{12}\}$ dense coacervates in response to temperature, $c_{e\{W12\}}/c_{SBMA}$, and c_{LiCl}.

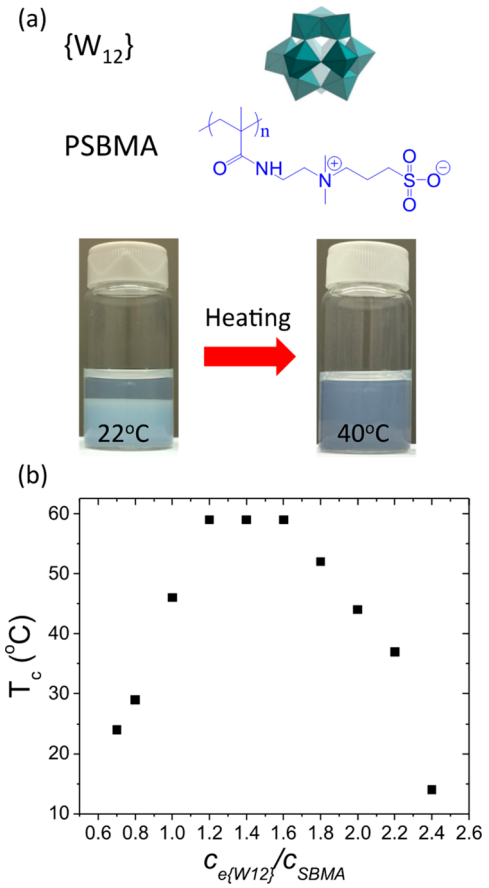

Figure 1. (a) Schematic illustration of molecular structure of $\{W_{12}\}$ and PSBMA and optical photographs to show the transition of biphasic PSBMA−$\{W_{12}\}$ coacervate complexes formed at c_{SBMA} = 85.5 mM, $c_{e\{W12\}}/c_{SBMA}$ = 220%, and c_{LiCl} = 0.5 M at T = 22 °C (left-side photograph) to monophonic complexes at T = 40 °C (right-side photograph). (b) Critical temperature, T_c, for the transition from biphasic coacervates to monophasic complexes against $c_{e\{W12\}}/c_{SBMA}$ for PSBMA−$\{W_{12}\}$ complexes formed at c_{SBMA} = 85.5 mM and c_{LiCl} = 0.5 M.

EXPERIMENTAL SECTION

PSBMA polymer was synthesized by strictly following the published procedure.[27] An aqueous solution of lithium metatungstate, $\{W_{12}\}$ ($Li_6H_2W_{12}O_{34}$), was purchased from LMT Liquid and freeze-dried (Labconco Freezone 4.5 Freeze-Dryer) before experiments.

To prepare dense PSBMA−$\{W_{12}\}$ coacervates for rheological measurements, the biphasic coacervate complexes were centrifuged (Sorvall Legend X1R Centrifuge, Thermo Scientific) at 22800g and 22 °C for at least 12 h to thoroughly remove the dilute supernatant phase from the dense coacervate phase. It is noted that no effect of centrifugal acceleration on the structure and rheological properties of

DOI: 10.1021/acs.macromol.8b01759
Macromolecules 2018, 51, 9405−9411

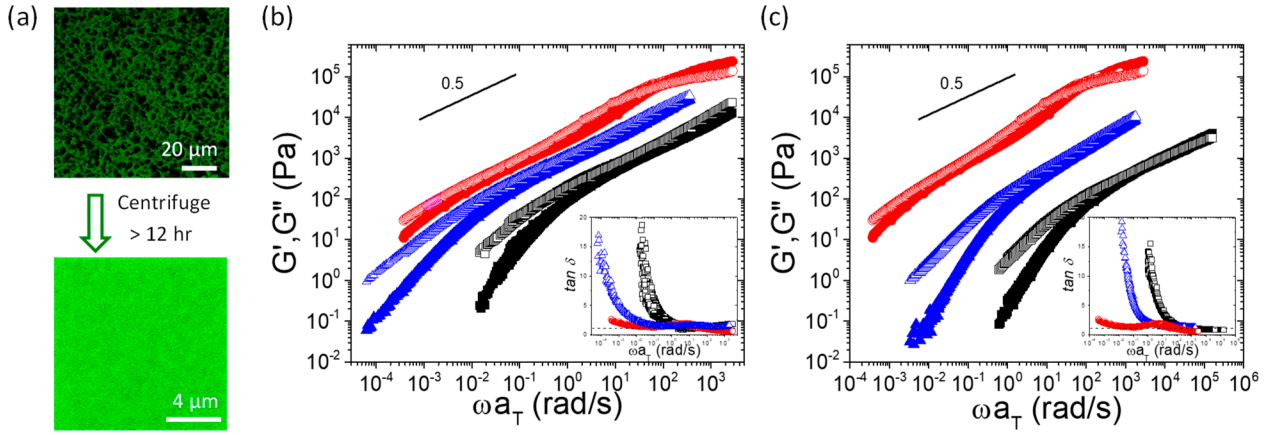

Figure 2. (a) Fluorescence micrographs of the morphology of PSBMA–$\{W_{12}\}$ dense coacervates formed at c_{SBMA} = 85.5 mM, $c_{e\{W12\}}/c_{SBMA}$ = 160%, and c_{LiCl} = 0.5 M and added with 5 mol % f-PSBMA before and after centrifugation. (b) Time–temperature superposition master curves of shear moduli G' (solid symbols) and G'' (open symbols) of PSBMA–$\{W_{12}\}$ dense coacervate against shifted angular frequency, ωa_T, for the coacervates formed at constant c_{SBMA} = 85.5 mM and c_{LiCl} = 0.5 M but varied $c_{e\{W12\}}/c_{SBMA}$ = 80% (black squares), 160% (red circles), and 200% (blue triangles). Inset: tan δ (= G''/G') of corresponding PSBMA–$\{W_{12}\}$ dense coacervates at varied $c_{e\{W12\}}/c_{SBMA}$. (c) Time–temperature superposition master curves of G' (solid symbols) and G'' (open symbols) of PSBMA–$\{W_{12}\}$ dense coacervate against shifted angular frequency, ωa_T, for the coacervates formed at constant c_{SBMA} = 85.5 mM and $c_{e\{W12\}}/c_{SBMA}$ = 160% but varied c_{LiCl} = 0.3 M (black squares), 0.4 M (blue triangles), and 0.5 M (red circles). Inset: tan δ of corresponding PSBMA–$\{W_{12}\}$ dense coacervates at varied c_{LiCl}.

dense coacervate was observed. The yielded dense coacervate is microscopically featureless as verified by super-resolution confocal laser scanning microscopy (CLSM, Carl Zeiss LSM 780) with a 63× objective lens (Plan-Apochromat, NA = 1.4, oil immersion) and an Airyscan detector (Carl Zeiss).

The linear viscoelasticity of PSBMA–$\{W_{12}\}$ dense coacervate was measured by a stress-controlled rheometer (Malvern Bohlin Gemni HRnano) with a parallel-plate fluid cell of 20 mm in diameter and 1000 μm in gap spacing. To prevent the slip of samples during shear, the surfaces of parallel plates were glued with sandpaper of grit size 600 (47185A51, Mcmaster-carr). After sample loading and achieving the desired gap spacing between the parallel plates, a thin film of paraffin oil (Aldrich) was applied to seal the edge of the sample to minimize the evaporation of water in samples. Linear shear spectra in response to applied frequency, ω = 0.19–62.8 rad/s, were obtained at constant shear strain, γ = 1%. Temperature was varied from 2 to 70 °C using a Peltier Element. For each temperature, a time period of 10 min was waited to ensure the sample reach the thermal equilibrium before measurements. Time–temperature superposition was performed for the frequency-dependent shear spectra of the dense coacervate samples based on the arbitrarily selected reference temperature of 42 °C.

FRAP was employed to examine the microstructure of dense coacervate complexes using CLSM. Fluorescein isothiocyanate–dextran (f-dextran, Sigma-Aldrich) of different M_w was used as the fluorescence probe and mixed with PSBMA aqueous solutions at a f-dextran concentration of ~10 μM before mixing with $\{W_{12}\}$. The measured $F(t)$ over the bleached circular area of d = 32 μm in diameter, normalized by that of the unbleached region of the same diameter, $F(0)$, was fitted by a one-phase exponential function using the "Bottom to (Span + Bottom)" analysis as $F(t)/F(0)$ = Bottom + Span*(1 − exp(−t ln 2/$\tau_{1/2}$)), where $\tau_{1/2}$ is the halftime for diffusion.[39] The apparent diffusion coefficient, D, of f-dextran in PSBMA–$\{W_{12}\}$ coacervates was obtained from $\tau_{1/2}$ according to D = $d^2/(4\tau_{1/2})$.

RESULTS AND DISCUSSION

Biphasic PSBMA–$\{W_{12}\}$ coacervate complexes are a thermodynamically stable system that can be formed over a wide range of $c_{e\{W12\}}/c_{SBMA}$ and c_{LiCl} at room temperature as previously reported.[27] Furthermore, we observe that the formation of biphasic PSBMA–$\{W_{12}\}$ coacervate complexes can be also modified by solution temperature, T. As shown in Figure 1a, a transition from biphasic to monophasic complexes as increasing T from 22 to 40 °C is clearly indicated by the photographs for the PSBMA–$\{W_{12}\}$ coacervate complex formed at c_{SBMA} = 85.5 mM, c_{LiCl} = 0.5 M, and $c_{e\{W12\}}/c_{SBMA}$ = 220%. It appears that the thermal responsive characteristics of PSBMA polyzwitterion persists in the hybrid coacervate complexes even though its upper critical solution temperature (UCST) decreases from ~45 °C in deionized water[35] to be below 0 °C in ionic aqueous solutions of either added LiCl concentration exceeding 50 mM or added $\{W_{12}\}$ concentration exceeding 1 mM found in this work. The critical temperature, T_c, at which a transition from biphasic coacervate to monophasic complex solution or hydrogel of PSBMA–$\{W_{12}\}$ complexes occurs is measured against varied $c_{e\{W12\}}/c_{SBMA}$ and c_{LiCl} at constant c_{SBMA} = 85.5 mM. T_c shows nonmonotonic dependence on $c_{e\{W12\}}/c_{SBMA}$ at constant c_{LiCl} = 0.5 M in Figure 1b. At $c_{e\{W12\}}/c_{SBMA}$ > 240%, T_c becomes immeasurable as the complexes exhibit a monophasic phase at T = 22 °C as previously reported.[27] The highest T_c is found at $c_{e\{W12\}}/c_{SBMA}$ ~ 160%, at which the measured linear viscoelasticity of dense coacervates is also peaked (see Figures 2 and 3). It is strongly suggested that the strongest interaction and network formation of PSBMA–$\{W_{12}\}$ coacervate complexes occur at the optimal $c_{e\{W12\}}/c_{SBMA}$ ~ 160% at given c_{SBMA} = 85.5 mM and c_{LiCl} = 0.5 M.

To examine the microstructural dynamics of PSBMA–$\{W_{12}\}$ dense coacervate complexes, we have characterized the frequency-dependent linear viscoelastic properties of dense coacervates at varied T (see Supporting Information Figures S1 and S2). For each dense coacervate sample, we have ensured that the supernatant, which might be dispersed in dense coacervate complexes in the form of submicrometer-sized droplets, is thoroughly removed by repeated centrifugation at 22800g for at least 12 h at T = 22 °C. Featureless and homogeneous morphology of PSBMA–$\{W_{12}\}$ dense coacervates is confirmed with fluorescein-labeled PSBMA (f-PSBMA) added in dense coacervates by super-resolution fluorescence microscopy as shown in Figure 2a. It should be

DOI: 10.1021/acs.macromol.8b01759
Macromolecules 2018, 51, 9405–9411

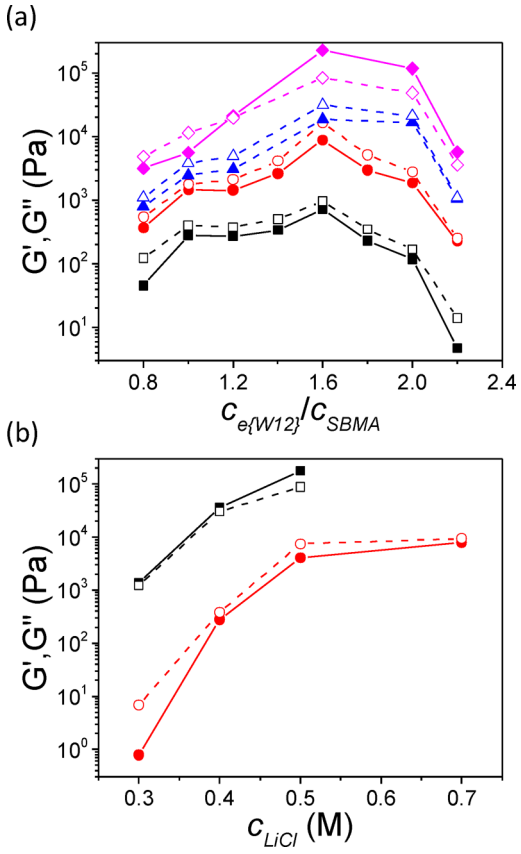

Figure 3. Effects of (a) $c_{e\{W12\}}/c_{SBMA}$ and (b) c_{LiCl} on linear storage moduli, G' (solid symbols), and loss moduli, G'' (open symbol), of PSBMA–$\{W_{12}\}$ dense coacervates measured at fixed angular frequency, ω = 6.28 rad/s, and strain, γ = 1%. In panel (a), the coacervates are formed at constant c_{SBMA} = 85.5 mM and c_{LiCl} = 0.5 M. Linear rheological data are shown at varied T = 58 °C (black squares), 42 °C (red circles), 34 °C (blue triangles), and 22 °C (magenta diamonds). In panel (b), the coacervates are formed at constant c_{SBMA} = 85.5 mM and $c_{e\{W12\}}/c_{SBMA}$ = 160%. Linear rheological data are shown at varied T = 26 °C (black squares) and 46 °C (red circles).

noted that the compositions of dense coacervates after centrifugation remain the same without any further phase separation even after the samples in sealed containers rest in the laboratory for several months. The actual concentrations of PSBMA, $\{W_{12}\}$, and LiCl in the coacervates vary with initial c_{SBMA}, $c_{e\{W12\}}/c_{SBMA}$, and c_{LiCl} in nonlinear fashion as detailed in our previous work;[27] thus, we have chosen to discuss the rheological properties of PSBMA–$\{W_{12}\}$ dense coacervates based on initial component concentration in solutions before coacervate formation. We have performed the standard analysis of time–temperature superposition to rescale all the linear frequency-dependent shear spectra (see Figure S3 for the T-dependent shifting factors a_T)[40] and obtain the master curves for PSBMA–$\{W_{12}\}$ dense coacervate against $c_{e\{W12\}}/c_{SBMA}$ and c_{LiCl} as shown in Figures 2b and 2c, respectively.

Strikingly, measured storage moduli, G', and loss moduli, G'', of all the dense coacervates overlap and both scale with $\omega^{0.5}$ against a substantial range of rescaled angular frequency, ωa_T, for nearly 6 orders of magnitude. Such linear viscoelastic spectra strongly suggest a critical gel behavior, which is loosely defined as a material state upon the sol–gel transition of viscoelastic materials.[41,42] Such an exceedingly broad spectrum of overlapping storage and loss moduli without a terminal relaxation time suggests the attribution of local PSBMA–$\{W_{12}\}$ gelation to their network structures.[43] In control, we have also characterized the viscoelastic behavior of simple PSBMA solution without $\{W_{12}\}$ at the same c_{LiCl} = 0.5 M but higher c_{SBMA} = 342 mM corresponding to the c_{SBMA} at which the highest shear moduli of dense coacervates are achieved in our system[27] (see Figure S4). The linear oscillatory frequency sweep results of $\{W_{12}\}$-free PSBMA solution exhibit the typical liquid-like behavior with predominantly larger G'' than G' over the entire frequency range, which is clearly distinct from those of PSBMA–$\{W_{12}\}$ dense coacervates. In addition, the measured shear moduli of PSBMA–$\{W_{12}\}$ dense coacervate are considerably enhanced by more than 5 orders of magnitude with added inorganic $\{W_{12}\}$ in comparison to those of $\{W_{12}\}$-free PSBMA/LiCl aqueous solutions. Thus, the significant enhancement in the viscoelasticity of PSBMA–$\{W_{12}\}$ dense coacervate strongly supports that the PSBMA–$\{W_{12}\}$ dense coacervates behave unlike a viscous solution but rather a monophasic hydrogel.

The measured G' and G'' of PSBMA–$\{W_{12}\}$ dense coacervates at varied T are summarized against $c_{e\{W12\}}/c_{SBMA}$ as shown in Figure 3a. Clearly, the nonmonotonic change of G' and G'' of PSBMA–$\{W_{12}\}$ dense coacervate shows the same trend as the change of T_c as well as the activation energy, E_a (see Table S1), with $c_{e\{W12\}}/c_{SBMA}$. Both shear moduli and T_c are peaked at $c_{e\{W12\}}/c_{SBMA} \sim 160\%$, strongly suggesting the presence of an optimal $c_{e\{W12\}}/c_{SBMA}$ for the maximal PSBMA–$\{W_{12}\}$ interaction and strongest network formation, despite being nonstoichiometric coacervates. It is also noted that the linear shear moduli of PSBMA–$\{W_{12}\}$ dense coacervates can be modified over 3 orders of magnitude by either $c_{e\{W12\}}/c_{SBMA}$ or T or both. Additionally, salt can also effectively modify the viscoelasticity of PSBMA–$\{W_{12}\}$ dense coacervates as shown in Figures 2c and 3b. Distinct from the salt-induced suppression of conventional polyelectrolyte coacervate complexation,[37] we have observed that increasing LiCl concentration can not only broaden the coacervate phase[27] but also considerably enhance the rheological strength of gel-like PSBMA–$\{W_{12}\}$ dense coacervates, i.e., the salt-hardening behavior as clearly exhibited in Figure 3b. Hence, such organic–inorganic macroion coacervate complexes evidently exhibit superior tunability in their viscoelastic properties by different environmental and solution conditions.

Distinct from the previously reported microstructures of polyelectrolyte dense coacervates in the literature,[18,38] we attribute the critical gel behavior and nonmonotonic $c_{e\{W12\}}/c_{SBMA}$ dependent viscoelasticity of PSBMA–$\{W_{12}\}$ dense coacervates to the competition between $\{W_{12}\}$ cross-linking and electrostatic repulsion between $\{W_{12}\}$-bound PSBMA. Multivalent $\{W_{12}\}$ could behave like a cross-linker due to its high binding affinity for the dipolar ionic groups of PSBMA. Because of the high multivalence of $\{W_{12}\}$ as polyanions, even when its concentration is low, one $\{W_{12}\}$ could bind with several PSBMA, giving rise to enhanced viscoelasticity of PSBMA–$\{W_{12}\}$ complexes in the solution phase. Increasing $c_{e\{W12\}}/c_{SBMA}$ in the coacervate phase regime could lead to the increased number of PSBMA–$\{W_{12}\}$ zwitterion–anion pairs upon biphasic coacervate formation, resulting in the increase of both volume fraction[27] of dense coacervate phase and T_c. On the other hand, the binding of $\{W_{12}\}$ to net neutral PSBMA leads to net negatively charged PSBMA–$\{W_{12}\}$ complexes. Thus, electrostatic repulsion among complexes could be much enhanced with increased $\{W_{12}\}$ concentration. As a result, the

DOI: 10.1021/acs.macromol.8b01759
Macromolecules 2018, 51, 9405–9411

effective number of cross-linking points could be greatly reduced with increased $\{W_{12}\}$ concentration, ultimately resulting in the decrease of viscoelasticity and T_c of coacervate complexes with further increased $c_{e\{W12\}}/c_{SBMA}$. Hence, an optimal $c_{e\{W12\}}/c_{SBMA}$ is present for the PSBMA−$\{W_{12}\}$ coacervate complexation at fixed c_{SBMA} and c_{LiCl} as indicated in Figure 3a.

To further verify the critical gel characteristics of dense coacervates, we examine the length scales of gel-like porous microstructures by the diffusion of fluorescein-labeled neutral dextran (f-dextran) with different molecular weight (M_w) as probes in PSBMA−$\{W_{12}\}$ dense coacervates using FRAP. We have ensured that f-dextran is a passive probe with negligible intermolecular attraction with PSBMA−$\{W_{12}\}$ dense coacervates in that the measured concentration of f-dextran in the supernatant phase is much higher than that in the coacervate phase (see Figure S5). Figure 4a shows the representative time-dependent fluorescence recovery profiles, $F(t)$, of f-dextran in PSBMA−$\{W_{12}\}$ dense coacervates formed at c_{SBMA} = 85.5 mM, $c_{e\{W12\}}/c_{SBMA}$ = 160%, and c_{LiCl} = 0.3 and 0.5 M in comparison to those in a homogeneous hydrogel formed at c_{SBMA} = 342 mM and $c_{e\{W12\}}/c_{SBMA}$ = 160% in LiCl-free aqueous solution and in deionized water as the control. For all the four cases, $F(t)$ can be well fitted with a one-phase exponential function[39] to yield a single diffusion coefficient, D, of f-dextran in different surroundings, in sharp contrast to the previously reported mesophase separation of polyelectrolyte coacervates with fast and slow probe diffusion.[18] The measured D of f-dextran for all the four different cases clearly exhibits a scaling with the M_w of f-dextran as shown in Figure 4b. The FRAP approach to investigate the averaged mesh pore size of a gel is based upon the fact that the diffusion of f-dextran in a homogeneous gel could resemble the Brownian motion of a spherical coil when f-dextran size is smaller than the average mesh size of the gel or the reptation motion of a "snake-like" chain when f-dextran size becomes comparable to or larger than the mesh size due to the confinement effect. Figure 4b evidently shows that the scaling of the measured D of f-dextran against M_w exhibits two distinct regimes: at low M_w, the scaling of $D \sim M_w^{-0.5}$ is observed with all the four cases and approximates to the Zimm behavior with the theoretically predicted exponent of −0.6;[44] yet at high M_w, the exponent is observed to be between −1 and −2, suggesting the approximation to the reptational behavior whose scaling is predicted to exhibit a power exponent of −2 for hydrogel.[44] In this work, we intend to determine the averaged mesh pore size of the gel-like dense coacervates from the critical hydrodynamic diameter of f-dextran, above which the scaling of D against M_w deviates from the Zimm behavior that is similar to the self-diffusion of dextran in free aqueous solution.[45] The deviation of the measured D from the Zimm behavior is found at the cutoff M_w of ∼20000 g/mol for the homogeneous hydrogel and ∼40000 and ≤4000 g/mol for the dense coacervate formed at c_{LiCl} = 0.3 and 0.5 M, respectively. Based on the dextran coil size corresponding to the measured cutoff M_w, the mesh pore size of dense coacervates is estimated to be 9.6 nm at c_{LiCl} = 0.3 M and ≤2.8 nm at c_{LiCl} = 0.5 M in comparison to the mesh size of 6.4 nm for the homogeneous gel formed without LiCl. The decrease of the mesh pore size of dense coacervates with increasing salt concentration is consistent with the salt-hardening viscoelasticity of PSBMA−$\{W_{12}\}$ dense coacervates observed in Figures 2c and 3b. Despite different mesh sizes possibly due to varied PSBMA−$\{W_{12}\}$ interactions, the dense coacervates exhibit the strikingly similar microstructures as a homogeneous gel.

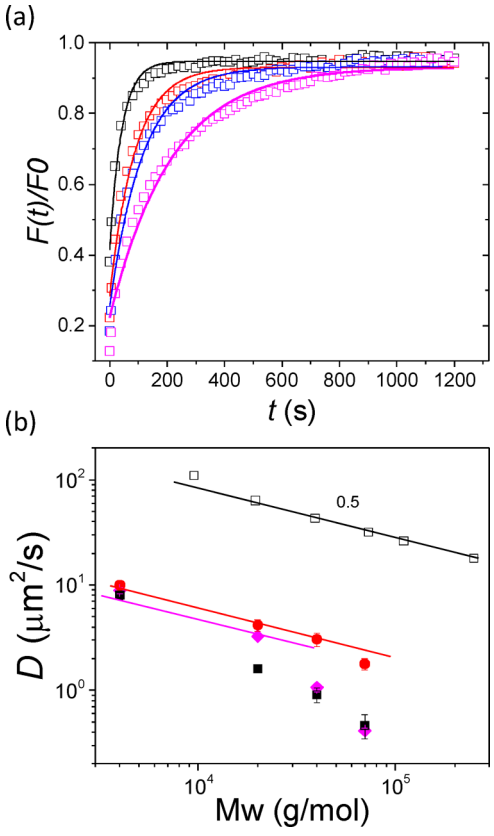

Figure 4. (a) Normalized fluorescence intensity recovery profile of FITC-labeled dextran (f-dextran) with different M_w = 4000 g/mol (black squares), 20000 g/mol (red circles), 40000 g/mol (blue triangles), and 70000 g/mol (magenta diamonds) against elapsed time, t, in PSBMA−$\{W_{12}\}$ dense coacervates formed at c_{SBMA} = 85.5 mM, $c_{e\{W12\}}/c_{SBMA}$ = 160%, and c_{LiCl} = 0.3 M at T = 22 °C. Solid lines are the fitting results using the one-phase exponential model. (b) M_w-dependent diffusion coefficient of f-dextran in free aqueous solution (black open squares) from previously published results (ref 45), homogeneous hydrogel of PSBMA−$\{W_{12}\}$ formed at c_{SBMA} = 342 mM and $c_{e\{W12\}}/c_{SBMA}$ = 160% without LiCl salt (magenta diamonds), and dense coacervate of PSBMA−$\{W_{12}\}$ formed at c_{SBMA} = 85.5 mM, $c_{e\{W12\}}/c_{SBMA}$ = 160%, and c_{LiCl} = 0.3 M (red circles) and 0.5 M (black squares). Solid lines are the fitting of results consistent with the Zimm model: $D \sim M_w^{-0.5}$.

CONCLUSIONS

In summary, we have reported the multiresponsive, critical gel-like behaviors of PSBMA−$\{W_{12}\}$ dense coacervates in response to varied $\{W_{12}\}$ and salt concentrations and temperature. Increasing temperature across T_c leads to the transition of PSBMA−$\{W_{12}\}$ complexes from biphasic coacervate complexes to monophasic solutions, where T_c strongly depends on $c_{e\{W12\}}/c_{SBMA}$. A similar nonmonotonic trend of T_c and shear moduli of dense coacervates against $c_{e\{W12\}}/c_{SBMA}$ indicates the presence of optimal $c_{e\{W12\}}/c_{SBMA}$ for the formation of the most stable and strongest PSBMA−$\{W_{12}\}$ dense coacervates. Moreover, linear rheological spectra of PSBMA−$\{W_{12}\}$ dense coacervates after thorough removal of the supernatants evidently indicate the unique critical gel behavior of the dense coacervates, where measured G' and G''

DOI: 10.1021/acs.macromol.8b01759
Macromolecules 2018, 51, 9405−9411

overlap and exhibit a scaling with $\omega^{0.5}$. To the best of our knowledge, it is for the first time that a critical gel-like complex can be simply formed via a coacervate complexation process. The viscoelasticity of dense coacervates is significantly enhanced by several orders of magnitude due to added POMs and can be further modified by added salt and temperature. The salt-hardening viscoelastic behavior is also distinct from salt suppression of conventional polyelectrolyte coacervates. To verify the gel-like microstructure, the averaged mesh pore sizes of PSBMA–$\{W_{12}\}$ dense coacervates are determined by f-dextran of increased M_w as passive molecular probes using FRAP in comparison to those in a homogeneous PSBMA–$\{W_{12}\}$ gel and a simple deionized water. The average mesh size of PSBMA–$\{W_{12}\}$ dense coacervates, determined from the cutoff dextran M_w where the deviation of measured dextran diffusion from the classical Zimm-like behavior occurs, is found to be <10 nm and decreases with increasing salt concentration. Hence, all the results strongly suggest the critical gel microstructure of PSBMA–$\{W_{12}\}$ dense coacervates, which possibly results from the cross-linking of PSBMA–$\{W_{12}\}$ zwitterion–anion pairs by excess $\{W_{12}\}$. In perspective, such hybrid organic–inorganic macroion coacervate complexes with significantly enhanced yet highly tunable viscoelasticity could open new avenues to design new "smart" functional nanomaterials for emerging applications from nanomedicines to environmental sustainability.

■ ASSOCIATED CONTENT

Supporting Information

The Supporting Information is available free of charge on the ACS Publications website at DOI: 10.1021/acs.macromol.8b01759.

Experimental details and additional supporting figures (PDF)

■ AUTHOR INFORMATION

Corresponding Authors

*(B.J.) Tel +1 313-577-3800; e-mail jingbenxin@gmail.com.
*(Y.Z.) Tel +1 313-577-1842; e-mail yzhu3@wayne.edu.

ORCID

Benxin Jing: 0000-0002-8400-1937
Donghua Xu: 0000-0003-1828-1210
Yingxi Zhu: 0000-0002-7968-1640

Notes

The authors declare no competing financial interest.

■ ACKNOWLEDGMENTS

B.J. and Y.Z. are grateful for the financial support from the National Science Foundation (NSF DMR-1743041) for this work.

■ REFERENCES

(1) Beijerinck, M. W. *Zentralblatt für Bakteriologie, Parasiten und Infektionskrankenheiten* **1896**, *2*, 697–699.
(2) Shin, Y.; Brangwynne, C. P. Liquid phase condensation in cell physiology and disease. *Science* **2017**, *357* (6357), No. eaaf4382.
(3) Stewart, R. J.; Wang, C. S.; Song, I. T.; Jones, J. P. The role of coacervation and phase transitions in the sandcastle worm adhesive system. *Adv. Colloid Interface Sci.* **2017**, *239*, 88–96.
(4) Zhao, H.; Sun, C.; Stewart, R. J.; Waite, J. H. Cement Proteins of the Tube-building Polychaete Phragmatopoma californica. *J. Biol. Chem.* **2005**, *280* (52), 42938–42944.
(5) Stewart, R. J.; Ransom, T. C.; Hlady, V. Natural Underwater Adhesives. *J. Polym. Sci., Part B: Polym. Phys.* **2011**, *49* (11), 757–771.
(6) Jia, T. Z.; Hentrich, C.; Szostak, J. W. Rapid RNA Exchange in Aqueous Two-Phase System and Coacervate Droplets. *Origins Life Evol. Biospheres* **2014**, *44* (1), 1–12.
(7) Jia, T. Z.; Fahrenbach, A. C.; Kamat, N. P.; Adamala, K. P.; Szostak, J. W. Oligoarginine Peptides Slow Strand Annealing and Assist Non-enzymatic RNA Replication. *Nat. Chem.* **2016**, *8* (10), 915–921.
(8) Ruiter, L. d.; Jong, H. G. B. d. The interfacial tension af gum arabic-gelatin camplex-coacervates and their equilibrium liquids. *Proc. Kon. Ned. Akad. Wetensch., Ser. B* **1947**, *50*, 836–848.
(9) Desmond, K. W.; Zacchia, N. A.; Waite, J. H.; Valentine, M. T. Dynamics of mussel plaque detachment. *Soft Matter* **2015**, *11* (34), 6832–6839.
(10) Lee, B. P.; Messersmith, P. B.; Israelachvili, J. N.; Waite, J. H. Mussel-Inspired Adhesives and Coatings. In *Annual Review of Materials Research*; Clarke, D. R., Fratzl, P., Eds., 2011; Vol. *41*, pp 99–132.
(11) Priftis, D.; Leon, L.; Song, Z.; Perry, S. L.; Margossian, K. O.; Tropnikova, A.; Cheng, J.; Tirrell, M. Self-Assembly of α-Helical Polypeptides Driven by Complex Coacervation. *Angew. Chem., Int. Ed.* **2015**, *54* (38), 11128–11132.
(12) Priftis, D.; Leon, L.; Song, Z.; Perry, S. L.; Margossian, K. O.; Tropnikova, A.; Cheng, J.; Tirrell, M. Self-Assembly of α-Helical Polypeptides Driven by Complex Coacervation. *Angew. Chem.* **2015**, *127* (38), 11280–11284.
(13) Li, L.; Yan, B.; Yang, J. Q.; Chen, L. Y.; Zeng, H. B. Novel Mussel-Inspired Injectable Self-Healing Hydrogel with Anti-Biofouling Property. *Adv. Mater.* **2015**, *27* (7), 1294–1299.
(14) Croguennec, T.; Tavares, G. M.; Bouhallab, S. Heteroprotein complex coacervation: A generic process. *Adv. Colloid Interface Sci.* **2017**, *239*, 115–126.
(15) Mason, A. F.; Buddingh', B. C.; Williams, D. S.; van Hest, J. C. M. Hierarchical Self-Assembly of a Copolymer-Stabilized Coacervate Protocell. *J. Am. Chem. Soc.* **2017**, *139* (48), 17309–17312.
(16) Yin, Y.; Niu, L.; Zhu, X.; Zhao, M.; Zhang, Z.; Mann, S.; Liang, D. Non-equilibrium behaviour in coacervate-based protocells under electric-field-induced excitation. *Nat. Commun.* **2016**, *7*, 10658.
(17) Fu, J.; Schlenoff, J. B. Driving Forces for Oppositely Charged Polyion Association in Aqueous Solutions: Enthalpic, Entropic, but Not Electrostatic. *J. Am. Chem. Soc.* **2016**, *138* (3), 980–990.
(18) Kayitmazer, A. B.; Bohidar, H. B.; Mattison, K. W.; Bose, A.; Sarkar, J.; Hashidzume, A.; Russo, P. S.; Jaeger, W.; Dubin, P. L. Mesophase Separation and Probe Dynamics in Protein-polyelectrolyte Coacervates. *Soft Matter* **2007**, *3* (8), 1064–1076.
(19) Chollakup, R.; Smitthipong, W.; Eisenbach, C. D.; Tirrell, M. Phase Behavior and Coacervation of Aqueous Poly(acrylic acid)–Poly(allylamine) Solutions. *Macromolecules* **2010**, *43* (5), 2518–2528.
(20) Qin, J.; Priftis, D.; Farina, R.; Perry, S. L.; Leon, L.; Whitmer, J.; Hoffmann, K.; Tirrell, M.; de Pablo, J. J. Interfacial Tension of Polyelectrolyte Complex Coacervate Phases. *ACS Macro Lett.* **2014**, *3* (6), 565–568.
(21) Carn, F.; Durupthy, O.; Fayolle, B.; Coradin, T.; Mosser, G.; Schmutz, M.; Maquet, J.; Livage, J.; Steunou, N. Assembling Vanadium(V) Oxide and Gelatin into Novel Bionanocomposites with Unexpected Rubber-like Properties. *Chem. Mater.* **2010**, *22* (2), 398–408.
(22) Carn, F.; Djabourov, M.; Coradin, T.; Livage, J.; Steunou, N. Influence of Decavanadate Clusters on the Rheological Properties of Gelatin. *J. Phys. Chem. B* **2008**, *112* (40), 12596–12605.
(23) Carn, F.; Steunou, N.; Djabourov, M.; Coradin, T.; Ribot, F.; Livage, J. First Example of Biopolymer-polyoxometalate Complex Coacervation in Gelatin-decavanadate Mixtures. *Soft Matter* **2008**, *4* (4), 735–738.
(24) Li, Y.; Tanaka, T. Phase transition of gels. *Annu. Rev. Mater. Sci.* **1992**, *22*, 243–277.

DOI: 10.1021/acs.macromol.8b01759
Macromolecules 2018, 51, 9405–9411

(25) Fratzl, P. Collagen: Structure and Mechanics, an Introduction. In *Collagen: Structure and Mechanics*; Fratzl, P., Ed.; Springer: Boston, MA, 2008; pp 1−13.
(26) Akyol, E.; Kirboga, S.; Öner, M. Polyelectrolytes: Science and Application. In *Polyelectrolytes: Thermodynamics and Rheology*; Visakh, P. M.; Bayraktar, O.; Picó, G. A., Eds.; Springer International Publishing: Cham, 2014; pp 87−112.
(27) Jing, B.; Qiu, J.; Zhu, Y. Organic-inorganic macroion coacervate complexation. *Soft Matter* **2017**, *13* (28), 4881−4889.
(28) Long, D.-L.; Burkholder, E.; Cronin, L. Polyoxometalate Clusters, Nanostructures and Materials: From Self Assembly to Designer Materials and Devices. *Chem. Soc. Rev.* **2007**, *36* (1), 105−121.
(29) Liu, T. Hydrophilic Macroionic Solutions: What Happens When Soluble Ions Reach the Size of Nanometer Scale? *Langmuir* **2010**, *26* (12), 9202−9213.
(30) Neumann, R. Polyoxometalate complexes in organic oxidation chemistry. *Prog. Inorg. Chem.* **1998**, *47*, 317−370.
(31) Hill, C. L.; Prosser-McCartha, C. M. Homogeneous catalysis by transition metal oxygen anion clusters. *Coord. Chem. Rev.* **1995**, *143*, 407−455.
(32) Lehmann, J.; Gaita-Ariño, A.; Coronado, E.; Loss, D. Spin qubits with electrically gated polyoxometalate molecules. *Nat. Nanotechnol.* **2007**, *2*, 312−317.
(33) Rhule, J. T.; Hill, C. L.; Judd, D. A.; Schinazi, R. F. Polyoxometalates in medicine. *Chem. Rev.* **1998**, *98*, 327−358.
(34) Hill, C. L.; Weeks, M. S.; Schinazi, R. F. Anti-HIV-1 activity, toxicity, and stability studies of representative structural families of polyoxometalates. *J. Med. Chem.* **1990**, *33*, 2767−2772.
(35) Mary, P.; Bendejacq, D. D.; Labeau, M.-P.; Dupuis, P. Reconciling Low- and High-Salt Solution Behavior of Sulfobetaine Polyzwitterions. *J. Phys. Chem. B* **2007**, *111* (27), 7767−7777.
(36) Jho, Y.; Yoo, H. Y.; Lin, Y.; Han, S.; Hwang, D. S. Molecular and structural basis of low interfacial energy of complex coacervates in water. *Adv. Colloid Interface Sci.* **2017**, *239*, 61−73.
(37) Liu, Y.; Winter, H. H.; Perry, S. L. Linear viscoelasticity of complex coacervates. *Adv. Colloid Interface Sci.* **2017**, *239*, 46−60.
(38) Marciel, A. B.; Srivastava, S.; Tirrell, M. V. Structure and rheology of polyelectrolyte complex coacervates. *Soft Matter* **2018**, *14*, 2454−2464.
(39) Schmid, J. A. http://www.meduniwien.ac.at/user/johannes.schmid/FRAPanalysis.htm.
(40) Larson, R. G. *The Structure and Rheology of Complex Fluids*; Oxford University Press: New York, 1999.
(41) Winter, H. H. The Critical Gel. In *Structure and Dynamics of Polymer and Colloidal Systems*; Borsali, R., Pecora, R., Eds.; Springer Netherlands: Dordrecht, 2002; pp 439−470.
(42) Rubinstein, M.; Colby, R. H. *Polymer Physics*; Oxford University Press: 2003.
(43) Winter, H. H.; Mours, M. Rheology of Polymers Near Liquid-Solid Transitions. In *Neutron Spin Echo Spectroscopy Viscoelasticity Rheology*; Springer: Berlin, 1997; pp 165−234.
(44) Pluen, A.; Netti, P. A.; Jain, R. K.; Berk, D. A. Diffusion of Macromolecules in Agarose Gels: Comparison of Linear and Globular Configurations. *Biophys. J.* **1999**, *77* (1), 542−552.
(45) Armstrong, J. K.; Wenby, R. B.; Meiselman, H. J.; Fisher, T. C. The Hydrodynamic Radii of Macromolecules and Their Effect on Red Blood Cell Aggregation. *Biophys. J.* **2004**, *87* (6), 4259−4270.

DOI: 10.1021/acs.macromol.8b01759
Macromolecules 2018, 51, 9405−9411